

Bursts of terahertz radiation from large-scale plasma irradiated by relativistic picosecond laser pulses

G. Q. Liao (廖国前)¹, Y. T. Li (李玉同)^{1,4*}, C. Li (李春)¹, L. N. Su (苏鲁宁)¹, Y. Zheng (郑轶)¹, M. Liu (刘梦)¹, W. M. Wang (王伟民)^{1,4}, Z. D. Hu (胡志丹)¹, W. C. Yan (闫文超)¹, J. Dunn², J. Nilsen², J. Hunter², Y. Liu (刘越)³, X. Wang (王瑄)¹, L. M. Chen (陈黎明)^{1,4}, J. L. Ma (马景龙)¹, X. Lu (鲁欣)¹, Z. Jin (金展)⁵, R. Kodama (兒玉了祐)⁵, Z. M. Sheng (盛政明)^{6,3,4*}, J. Zhang (张杰)^{3,4}

¹ *Beijing National Laboratory for Condensed Matter Physics, Institute of Physics, Chinese Academy of Sciences, Beijing 100190, China*

² *Lawrence Livermore National Laboratory, 7000 East Avenue, Livermore, CA 94551, USA*

³ *Key Laboratory for Laser Plasmas (MoE) and Department of Physics and Astronomy, Shanghai Jiao Tong University, Shanghai 200240, China*

⁴ *IFSA Collaborative Innovation Center, Shanghai 200240, China*

⁵ *Photon Pioneers Center, Osaka University, 2-1 Yamada-oka, Suita, Osaka, 565-0871, Japan*

⁶ *SUPA, Department of Physics, University of Strathclyde, Glasgow G4 0NG, UK*

Powerful terahertz (THz) radiation is observed from large-scale underdense preplasma in front of a solid target irradiated obliquely with picosecond relativistic intense laser pulses. The radiation covers an extremely broad spectrum with about 70% of its energy located in the high frequency regime over 10 THz. The pulse energy of the radiation is found to be above 100 μJ per steradian in the laser specular direction at an optimal preplasma scale length around 40~50 μm . Particle-in-cell simulations indicate that the radiation is mainly produced by linear mode conversion from electron plasma waves, which are excited successively via stimulated Raman scattering instability and self-modulated laser wakefields during the laser propagation in the preplasma. This radiation can be used not only as a powerful source for applications, but also as a unique diagnostic of parametric instabilities of laser propagation in plasma.

PACS number: 52.59.Ye, 52.38.Kd, 52.25.Os

* To whom correspondence should be addressed. Email: ytli@iphy.ac.cn and zmscheng@sjtu.edu.cn.

The terahertz (THz) radiation, which lies between far infrared wave and microwave in the electromagnetic spectrum, has attracted increasing interest over the last decades for its wide range of promising applications [1,2]. One of the key issues for applications is to produce THz radiation sources with high power. A variety of schemes for THz radiation generation have been demonstrated. For example, the tilted-pulse-front pumping optical rectification is found to be an efficient scheme [3]. However, the damage threshold for nonlinear optical materials prevents the use of high pumping laser intensity for high THz power. In contrast, a plasma medium does not have such a limitation and has the potential to generate more powerful THz emission [4]. For example, Leemans *et al.* reported THz emission at 3-5 $\mu\text{J}/\text{sr}$ from laser wakefield-accelerated electron bunches passing through a plasma-vacuum boundary [5]. Sheng *et al.* proposed that THz emission can be produced directly from laser wakefields driven in inhomogeneous plasma via linear mode conversion (LMC) [6]. THz generation from air-plasma filaments produced with moderate intense lasers has also been investigated extensively [7,8,9,10]. In this case, the two-color laser field scheme is usually more efficient with the energy conversion efficiency as high as 10^{-3} [11,12,13,14], although the THz radiation tends to saturate with increasing pump laser energy [12].

In the recent years, considerable attention has been paid to THz radiation from relativistic laser-solid interaction, which is supposed to have the potential for stronger radiation. THz radiation with energy $> \mu\text{J}/\text{pulse}$ from femtosecond laser-solid interactions has been observed either from the front [15,16,17] or the rear surface [18]. Several mechanisms responsible for the radiation have been proposed, *e.g.*, the transient electrons current driven by ponderomotive force [15], the “antenna” model [16], the surface electron current model [17], and dipole-like radiation originated from the target normal sheath field [18]. These models are generally based upon the electron currents produced at the target surface. Meanwhile, it has been found that preplasma is of great importance for THz radiation [19].

In this Letter, we study the THz radiation from a solid target in a different regime, where a relativistic *picosecond* laser pulse interacts with a *large-scale* inhomogeneous preplasma created by amplified spontaneous emission (ASE) and controlled prepulses in advance of the main laser pulse. By optimizing the preplasma scale lengths, THz radiation with energies up to above 100 $\mu\text{J}/\text{sr}$ level

is observed. Our particle-in-cell (PIC) simulations indicate that strong electron plasma waves (EPWs) are first excited by stimulated Raman scattering (SRS) and successively by self-modulated laser wakefields (SM-LWF). The EPWs are subsequently converted into THz radiation through the LMC mechanism. This wave-based process is fundamentally different from other current-based mechanisms reported so far.

The experiments were carried out using the COMET laser system [20] at the Lawrence Livermore National Laboratory (LLNL). It can deliver 1053 nm laser pulses with a maximum energy of 10 J and pulse duration of 0.5 ps. Figure 1 shows a schematic view of the experimental setup. A collimated *p*-polarized main laser pulse was focused onto a ~ 1 mm thick copper target at an incidence angle of 62.5° using an off-axis parabolic (OAP) mirror. The focal spot diameter was ~ 7 μm , giving an equivalent irradiance of $\sim 5 \times 10^{17}$ W/cm^2 for 1 J laser energy. The laser contrast was $\sim 10^5$. To generate a controllable and quasi one-dimensional preplasma, an off-collimated prepulse of 0.5 ps at 1053 nm, propagating coaxially with the main pulse, was also focused onto the target with the same OAP. The focal spot of the prepulse was much larger, ~ 100 μm in diameter, due to the off-collimation. The scale length of the preplasma was adjusted by changing the energy of the prepulse or the time delay between the main laser pulse and the prepulse. A Nomarski interferometer with a 0.5 ps, 527 nm laser pulse as a probe beam was used to measure the density profile of the preplasma. The timing of probe was set at 60 ps before the main pulse.

THz radiation was measured with a pyroelectric detector in the specular (62.5°) direction. A THz lens, made of polymethylpentene, was used to collect the radiation. The collimated THz emission transmitted through a THz window and was then refocused by another THz lens onto the detector. HRFZ-Si, Teflon and plastic filters were put before the detector, which transmit THz radiation, block scattered laser light and visible light, and avoid the saturation of the detector as well. The measured frequency range was from 0.1 THz, limited by the pyroelectric detector, to 250 THz, limited by the Si filters. The effective responsivity of the combination of the filters and detector is also shown in Fig. 1.

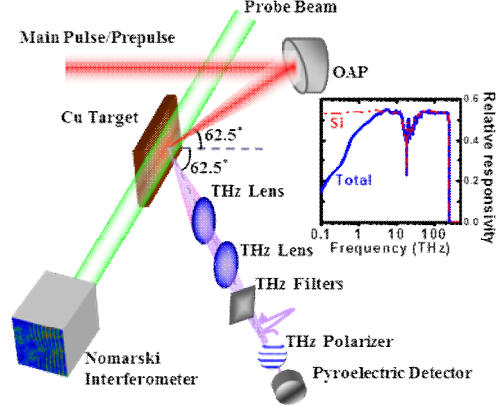


FIG. 1 (color online). Schematic view of the experimental setup. The inset shows the transmittance curve of HRFZ-Si calibrated with a Fourier transform infrared spectrometer (red dash dotted) and the total effective responsivity of the combination of the filters and detector (blue solid).

We have measured the THz pulse energy as a function of the main laser energy E_{laser} , and the preplasma scale length L , systematically. The dependence of the THz energy on E_{laser} is shown in Fig. 2(a). The radiation increases nonlinearly with E_{laser} . By increasing E_{laser} from 4 J to 9 J, the THz signal is enhanced by ~ 30 times. If fitting the data with a power law, the corresponding power index is $\sim 3 \pm 0.5$. For $E_{laser} = 9$ J, the THz energy is up to $11.5 \mu\text{J}$ in 0.05 sr, corresponding to 0.23 mJ/sr. There is no evidence of saturation of THz radiation with E_{laser} .

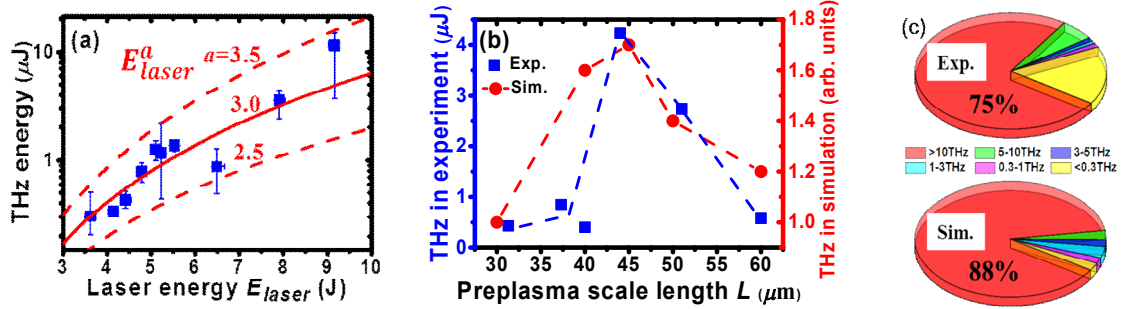


FIG. 2 (color online). Dependence of the THz energy or relative THz intensity on (a) the laser energy, (b) preplasma scale length L , and (c) different frequency regions. The experimental data is an average of about 5 shots. The data in (b) and (c) are obtained at $E_{laser} \sim 5$ J with a shot-to-shot fluctuation of 10%.

Figure 2(b) shows the THz radiation versus L , defined as $L = [(1/n_e)(dn_e/dx)]^{-1}$, where the direction x is the normal to the target. The electron density n_e can be obtained by Abel inversion of the interferograms. We can see the THz radiation is very sensitive to L . When L increases from $\sim 30 \mu\text{m}$ to $\sim 45 \mu\text{m}$, the THz radiation is enhanced by ~ 8 times. When L increases to $\sim 60 \mu\text{m}$, it

dramatically drops back to the level comparable to the case at $L \sim 30 \mu\text{m}$. Obviously, there exists an optimal L for the THz radiation.

Typically, the *spectral encoding* technique is used to measure the waveform and spectrum of THz radiation driven by femtosecond laser pulses running at a high repetition rate [17,21,22]. However, this technique does not work well for THz radiation driven by picosecond lasers since the long pulse width results in very poor temporal resolution and the narrow bandwidth makes it difficult to be chirped. The high frequency detection cutoff for a nonlinear crystal like ZnTe is another limitation [23]. Therefore, to estimate the frequency spectrum, a set of low-pass multi-mesh filters with cut-off frequency at 10, 5, 3, 1, 0.3 THz were set in front of the pyroelectric detector. Figure 2(c) shows the relative energy proportion of THz radiation in different frequency regions. Besides the small low-frequency component, most of the THz radiation ($\sim 75\%$ of the total energy) goes to the region >10 THz. Moreover, a wire-grid polarizer was used in the experiment to measure the polarization of THz radiation. The THz radiation behaves like a p -polarized pulse, which is similar as found before [15,17].

The previously proposed models for THz radiation from laser-solid interactions cannot well explain the above results. For example, the observed THz frequency is much higher than the predicted frequency by the “antenna” model [16] for the $10 \text{ mm} \times 20 \text{ mm}$ targets we used. The surface current model does not work due to the disappearance of surface fast electrons in a large-scale preplasma [17]. The target normal sheath field emission mechanism [18] works only for the radiation from the rear target surface.

On the other hand, it has been proposed by Sheng *et al.* that strong THz radiation can be produced via LMC when large-amplitude laser wakefields are excited by an ultrashort intense laser pulse obliquely incident into a nonuniform underdense plasma at the density around $10^{16-18} \text{ cm}^{-3}$ (corresponding to 1-10 THz) [6]. According to this theory, EPWs at different positions can emit electromagnetic waves at local plasma frequencies. Therefore, THz radiation with a broad frequency range may be produced. In the present case, even though there is a large nonuniform preplasma, the laser pulse duration in our experiments is so long (0.5 ps) that large-amplitude laser wakefields with high frequency (higher than 2 THz) cannot be driven directly by the laser

ponderomotive force. However, there are still two ways to excite large-amplitude EPWs by a long laser pulse. One is the self-modulated laser wakefields (SM-LWF) excitation, which occurs as a result of relativistic self-modulation instability (SMI) [24,25]. Another is by stimulated Raman backward scattering (SRBS), which occurs spontaneously during the laser propagation in a large-scale plasma [26]. Figure 3 illustrates schematically the involved processes, where EPWs driven by both processes can be partially converted into electromagnetic waves in the THz range via the LMC mechanism.

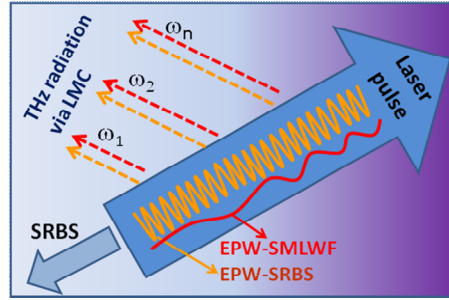


FIG. 3 (color online). Schematic diagram showing the THz radiation via LMC in a nonuniform plasma. When the intense picosecond laser pulse is incident obliquely into a nonuniform underdense plasma, EPWs are produced in a wide region along the laser propagation by SRBS and SM-LWF. Note even though these two kinds of EPWs show distinctly different wavelengths, but the radiation frequency is determined by the local plasma frequency.

To demonstrate those processes, we have conducted one-dimensional PIC simulations with similar laser and plasma conditions to the experimental. A sine-square-profiled laser pulse with a normalized peak amplitude $a_0=1.5$ and a pulse duration $\tau_L=150\tau_0$, is incident onto a plasma slab at an angle of $\theta=60^\circ$, where a_0 is related to the laser intensity I_0 and wavelength λ_0 by $a_0^2=I_0 \lambda_0^2/(1.37 \times 10^{18} \text{W/cm}^2)$, and τ_0 is the laser cycle. The plasma density is described by an exponential function along the x -direction with the scale length L , where the minimum and maximum density are set to be $0.0004n_c$ and $0.04n_c$, respectively, where n_c is the critical density of the pump laser. In order to deal with the oblique incidence of the laser pulse, a boosted frame moving with a speed $c \sin \theta$ along y direction is adopted [27]. Figure 4 shows typical simulation results, where p -polarized strong electromagnetic waves are found to be emitted from the left boundary of the plasma slab. Here we set the incident laser pulse to be s -polarized to avoid the possible mixture between the radiation from LMC and the scattered or reflected light from the laser

pulse. Figure 4(a) shows the spatial-temporal evolution of transverse field (THz radiation field). It is found that the generation of THz radiation can be divided into three time windows: $<75\tau_0$, $75-450\tau_0$, $>450\tau_0$ (see below), which correspond to three distinct radiation frequency spectra. The integrated frequency spectra of the THz emission and backward scattered light for the three stages are shown in Figs. 4(b-d) and 4(e-f), respectively.

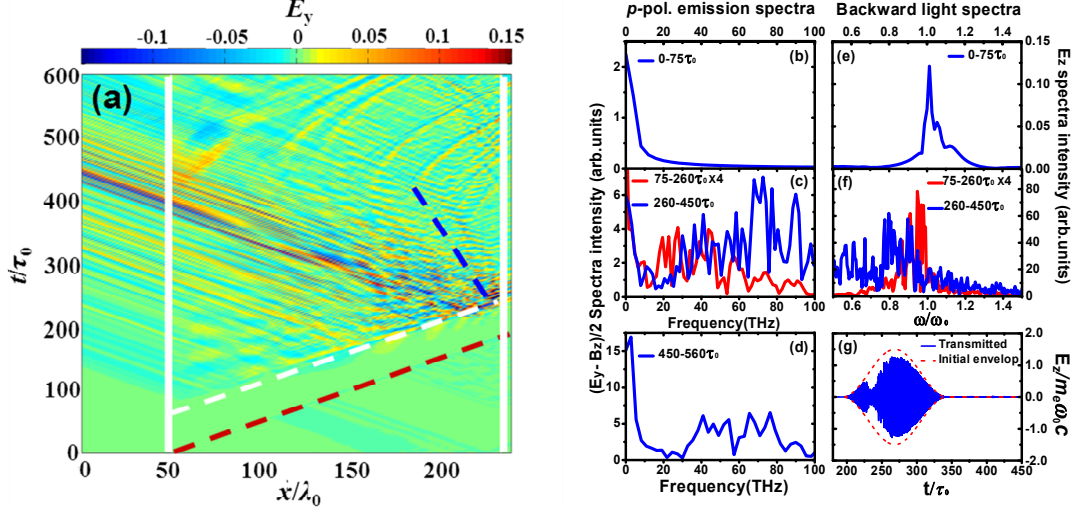


FIG. 4 (color online). (a) Spatial-temporal plots of the THz radiation field from PIC simulations. The plasma density rises exponentially from $x=50\lambda_0$ to $x=234\lambda_0$ with $L=40\lambda_0$. The white solid lines show the vacuum-plasma boundary. The laser pulse runs along $t=x$, indicated by the red dashed line. The white dashed line shows $t=x+\tau_L/2$. The time-integrated frequency spectra of (b-d) the p -polarized THz emission and (e-f) backward scattered laser light in different temporal stages, detected at $x=45\lambda_0$ in vacuum. (g) The waveform of the laser pulse transmitting the plasma slab, detected at $x=244\lambda_0$, and the initial envelop of laser pulse. The spectrum for $75-260\tau_0$ has been multiplied by a factor of 4.

When the laser pulse just goes into the plasma, a small part of laser is reflected and weak single-cycle low-frequency THz emission is observed from the left vacuum-plasma interface. The radiation can be explained by the transient currents at the vacuum-plasma interface driven by the laser pulse front, where the plasma density is very low [28]. Figure 4(b) and 4(e) show the time-integrated THz frequency spectrum and backward scattered light over $0-75\tau_0$. The radiation from this stage is very small and can be neglected in the present case.

When the laser pulse propagates deep into the plasma with higher densities, multi-cycle p -polarized THz radiation is generated. It is found that this radiation is closely associated with the

SRBS instability developed with the laser pulse propagation in the large-scale underdense preplasma. Figure 4(f) shows clearly that the scattered light is red-shifted, and it becomes stronger at later time when the laser pulse propagates into higher-density plasma. While the central frequency of the scattered light decreases with time, the central frequency of THz radiation increases with time (as a positive-chirp pulse). Note that the sum of the central frequency of the THz radiation and that of the scattered light is kept close to the laser frequency ω_0 at different time. This convinces us that the THz radiation is converted from the SRBS-induced plasma waves through the LMC mechanism. The SRBS is greatly enhanced near the intensity peak of laser pulse, and excites large-amplitude plasma waves, which provide a strong source for the LMC process. This is why the mode conversion occurs along near $t=x+\tau_L/2$, as indicated by the white dashed line in Fig. 4(a). Note that the positive-chirp THz radiation is also an important signature of LMC [6]. Therefore, we conclude that the second stage of THz radiation is caused by the combined SRBS and LMC processes.

With the further laser propagation, self-modulation instability starts to develop. This is because the relativistic self-modulation instability develops much more slowly than SRBS instability [25]. The waveform of the laser pulse transmitting the plasma slab is shown in Fig. 4(g), where the red dashed line is the initial laser envelope. The waveform is obviously imposed with many burr structures. The deep self-modulation even breaks the laser pulse into multi-pulses. Self-modulation instability leads to the excitation of SM-LWF. In our simulations, strong wakefields are generated near $t=d_{plasmas}+\tau_L/2$, where $d_{plasmas}$ represents the longitudinal size of plasmas. LMC from SM-LWF to THz radiation occurs where the phase velocity of wakefields changes its sign, marked by the blue dashed line in Fig. 4(a). The converted THz radiation is detected after about $t=2d_{plasmas}+\tau_L/2$ in vacuum. As shown in Figs. 4(d), the THz central frequency is about $0.2\omega_0$, well corresponding to the plasma frequency of the maximum density $0.04n_c$. Meanwhile, no backward scattered laser light is observed because the laser pulse has passed through the plasma. Therefore, THz radiation in the third stage is caused by SM-LWF and LMC.

The above model can explain most of the observed features of THz radiation. Figure 2(b) also shows the THz energy dependence on L from the simulations. We can see that there is an optimized scale length $L_{optimal}$ at which the THz radiation is the most efficient, in agreement with experiments.

According to the LMC model, there exists an optimal inhomogeneous configuration for a given incidence angle. It is observed to be $\sim 45 \mu\text{m}$ both in the experiment and in the simulation.

In the LMC model, the THz frequency is equal to the local plasma frequency and its distribution depends mainly on the plasma density profile. For the EPWs excitation either via SRBS or SM-LWF, their growth rates increase with the plasma density. This implies EPWs excited in the relatively high density region are predominant and the radiation via LMC is also predominant there. In our experiment, the density of preplasma region where the laser-plasma interaction mainly occurs is higher than 10^{18} cm^{-3} , which corresponds to a plasma frequency larger than 9 THz. This is also consistent with our observations and simulations, as shown in Fig. 2(c).

Finally, the scale length L is measured to be $\sim 30 \mu\text{m}$ in the experiment for the laser energy of 5 J even without the introduced prepulse. When the laser energy is increased from 5 J to 10 J, L will become larger and close to the L_{optimal} , leading to an increasing conversion efficiency. Moreover, the instability growth rates for SRBS and SMI increase with the laser intensity. This can explain qualitatively why the THz radiation observed in experiments increases rapidly with the laser energy, as shown in Fig. 2(a). In addition, our theory model indicates that the radiation is always p -polarized. This is also in agreement with the observed.

It is worthwhile to compare the present THz radiation with that produced by femtosecond laser-solid interactions where a small-scale preplasma with a steep density gradient is formed [17,19]. The energy of picosecond laser-driven THz pulses here is found to be higher than that of femtosecond laser-driven THz pulses [17], even though its energy conversion efficiency from the laser to THz radiation is lower. Nevertheless, the efficiency could be further improved by enhancing the EPW amplitude in some controlled ways [29,30,31]. The new mechanism presented here could also be applied to the gas or cluster targets, where the spectra of THz radiation are potentially tunable by tailoring the gas density.

The present THz radiation mechanism may also provide an alternative diagnostic of parametric instabilities of laser propagation in plasma. By measuring the THz radiation, one may estimate the saturation level of excited EPWs, which will help to understand the mechanisms of saturation of

parametric instabilities, a topic of significant interest and importance for inertial confined fusion [32].

We wish to thank the Jupiter laser facility team at LLNL for laser operation and technical support, and K. Wang, X. G. Qiu at the National Laboratory for Superconductivity in Beijing for calibrating the transmittance of filters. This work is supported by the National Basic Research Program of China (Grant Nos. 2013CBA01501 and 2014CB339801), the National Nature Science Foundation of China (Grant Nos. 11135012, 11375262, 11105217, 11421064, 11129503 and 11375261). Part of this work performed is under the auspices of the U.S. Department of Energy by LLNL under Contract No. DE-AC52-07NA27344.

References

-
- [1] M. S. Sherwin *et al.*, Editors, Opportunities in THz Science Report of a DOE-NSF-NIH Workshop held February 12-14, 2004, Arlington, VA.
 - [2] M. Tonouchi, *Nat. Photonics* **1**, 97 (2007).
 - [3] J. Hebling *et al.*, *Opt. Express* **10**, 1161 (2002); H. Hirori *et al.*, *Appl. Phys. Lett.* **98**, 091106 (2011); J. A. Fülöp *et al.*, *Opt. Lett.* **37**, 557 (2012).
 - [4] Y. T. Li *et al.*, *Chin. Phys. B* **21**, 95203 (2012).
 - [5] W. P. Leemans *et al.*, *Phys. Rev. Lett.* **91**, 074802 (2003).
 - [6] Z. M. Sheng *et al.*, *Phys. Rev. Lett.* **94**, 095003 (2005); Z. M. Sheng *et al.*, *Phys. Plasmas* **12**, 123103 (2005).
 - [7] P. Sprangle *et al.*, *Phys. Rev. E* **69**, 066415 (2004).
 - [8] X. Xie *et al.*, *Phys. Rev. Lett.* **96**, 075005 (2006).
 - [9] C. D'Amico *et al.*, *Phys. Rev. Lett.* **98**, 235002 (2007).
 - [10] A. Houard *et al.*, *Phys. Rev. Lett.* **100**, 255006 (2008).
 - [11] D. J. Cook and R. M. Hochstrasser, *Opt. Lett.* **25**, 1210 (2000); M. Kress *et al.*, *Opt. Lett.* **29**, 1120 (2004).
 - [12] K. Y. Kim *et al.*, *Nat. Photonics* **2**, 605 (2008).
 - [13] W. M. Wang *et al.*, *Phys. Rev. E* **87**, 033108 (2013).
 - [14] M. Clerici *et al.*, *Phys. Rev. Lett.* **110**, 253901 (2013).
 - [15] H. Hamster *et al.*, *Phys. Rev. Lett.* **71**, 2725 (1993); H. Hamster *et al.*, *Phys. Rev. E* **49**, 671(1994).

-
- [16] A. Sagiska *et al.*, Appl. Phys. B **90**, 373 (2008).
- [17] Y. T. Li *et al.*, Appl. Phys. Lett. **100**, 254101 (2012).
- [18] A. Gopal *et al.*, New J. Phys. **14**, 083012 (2012); A. Gopal *et al.*, Phys. Rev. Lett. **111**, 074802 (2013); A. Gopal *et al.*, Opt. Lett. **38**, 4705 (2013).
- [19] C. Li *et al.*, Phys. Rev. E **84**, 036405 (2011); C. Li *et al.*, Opt. Express **22**, 11797 (2014).
- [20] J. Dunn *et al.*, Opt. Lett. **24**, 101 (1999).
- [21] Z. Jiang and X.-C. Zhang, Appl. Phys. Lett. **72**, 1945 (1998).
- [22] N. H. Matlis *et al.*, J. Opt. Soc. Am. B **28**, 23 (2011).
- [23] Q. Wu *et al.*, Appl. Phys. Lett. **68**, 2924 (1996).
- [24] N. E. Andreev *et al.*, JETP Lett. **55**, 571 (1992); P. Sprangle *et al.*, Phys. Rev. Lett. **69**, 2200 (1992); T. Antonsen and P. Mora, Phys. Rev. Lett. **69**, 2204 (1992); A. Modena *et al.*, Nature **337**, 606 (1995).
- [25] C. D. Decker *et al.*, Phys. Plasmas **3**, 2047 (1996).
- [26] W. L. Kruer, *The Physics of Laser Plasma Interactions* (Addison-Wesley, New York, 1988).
- [27] R. Lichters *et al.*, Phys. Plasmas **3**, 3425 (1996).
- [28] Z. M. Sheng *et al.*, Phys. Rev. E **69**, 025401 (2004); H. C. Wu *et al.*, Phys. Rev. E **77**, 046405 (2008).
- [29] Y. Kitagawa *et al.*, Phys. Rev. Lett. **68**, 48 (1992).
- [30] Z. M. Sheng *et al.*, Phys. Plasmas **9**, 3147 (2002).
- [31] G. Shvets *et al.*, Phys. Rev. E **60**, 2218 (1999).
- [32] B. J. Winjum *et al.*, Phys. Rev. Lett. **110**, 165001 (2013).